Melting at the Core-Mantle Boundary and the Topography of the Ultralow Velocity Zone

Sash Hier-Majumder

CIDER workshop, June, 2008

Ultralow velocity zone at the core-mantle boundary

- Thickness varies between 5-40 km
- Estimated melt volume fraction between 5-30%
- Logarithmic ratio of seismic velocities vary between 2.5-3.2

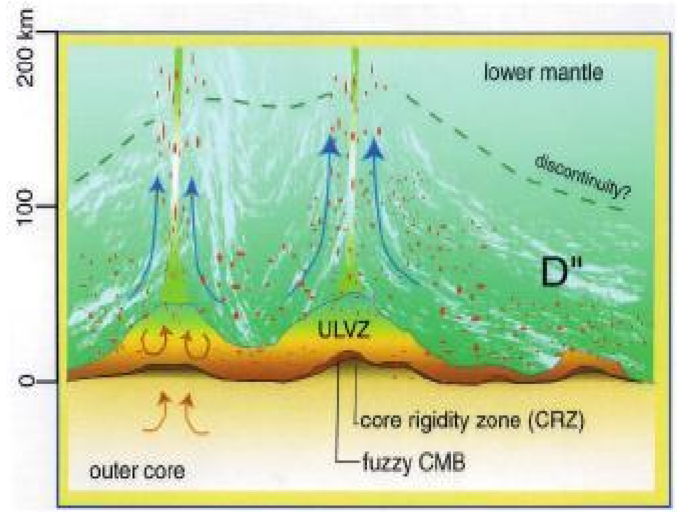

Garnero *[2004]*

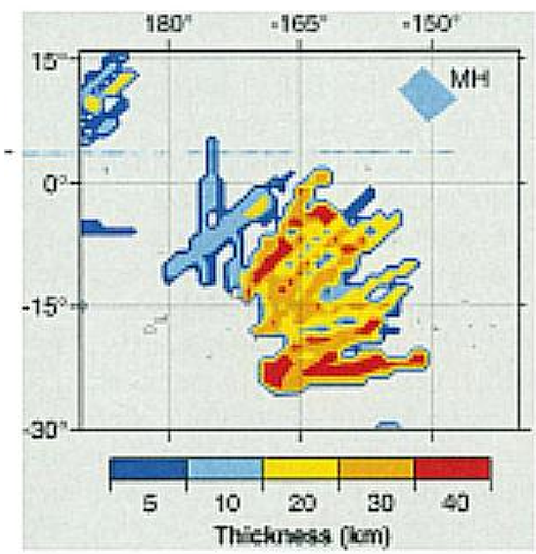

Williams and Garnero *[1996]*

Structure of the basal layer

- Lateral variation in topography
- Lower viscosity compared to the mantle
- Low seismic velocity

Jellinek and Manga *[2004*]

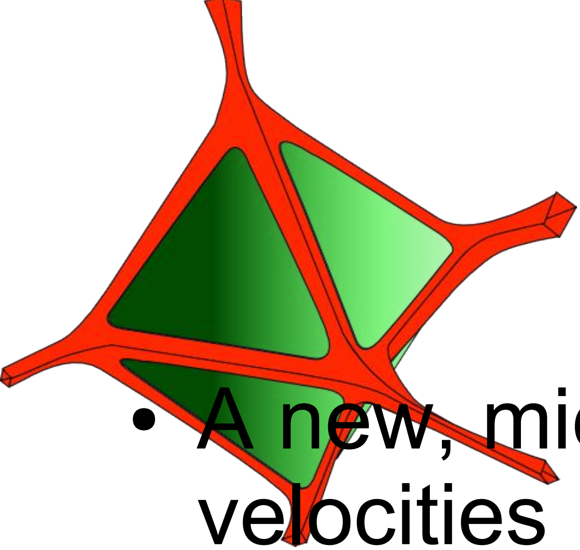

Outline

- A new, microstructure based, model for seismic velocities
- Estimated melt volume fraction at the ULVZ
- Influence of surface tension on the topography of the ULVZ
- Influence of viscosity contrast on the topography of the ULVZ

Microstructure modeling

- Elastic wave velocities in two-phase media is controlled by the area of contact or contiguity between adjacent particles [*Takei, 1998, 2000*].
- Steady-state contiguity is achieved by viscous sintering of the multiphase aggregate

Disaggregation

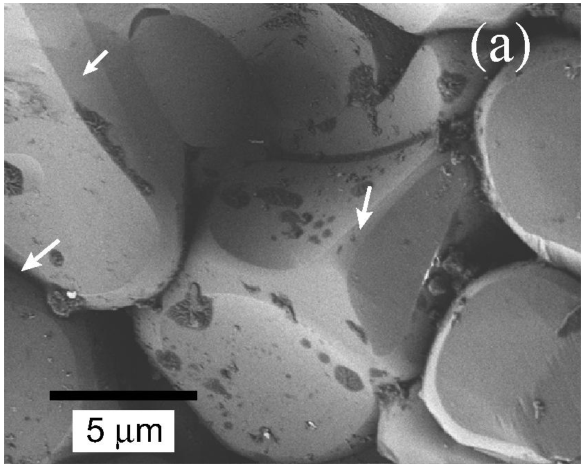

Hier-Majumder *et al. [2005]*

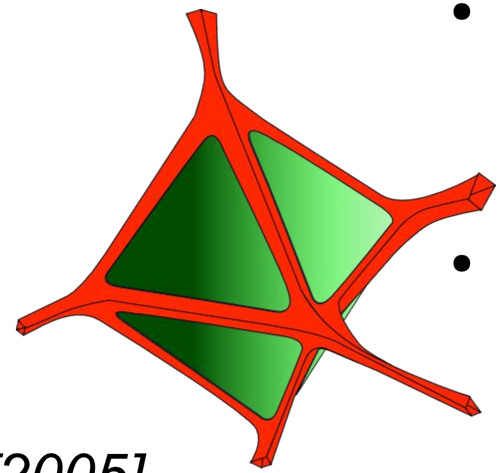

- Grains are contiguous at melt fractions below the disaggregation melt fraction
- At higher melt fractions, grains are suspended in the melt

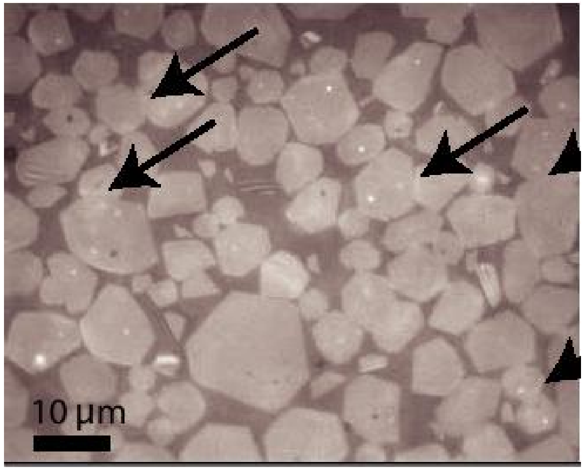

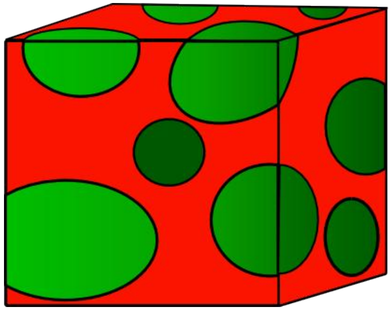

Scott and Kohlstedt *[2006]*

Interfaces in rocks

$$\chi = A_{gg}\gamma_{gg} + A_{gm}\gamma_{gm}$$

$$\psi = \frac{A_{gg}}{A_{gg} + A_{gm}}$$

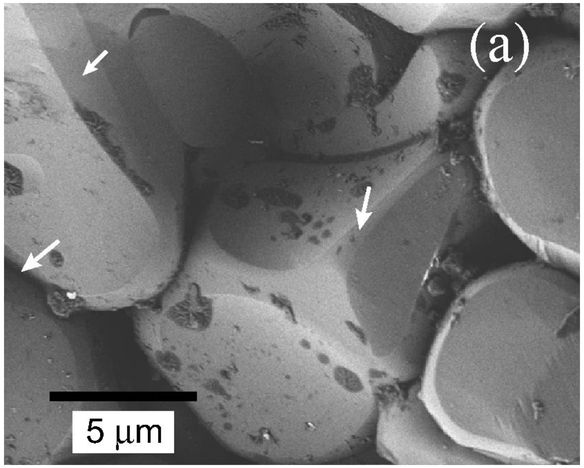

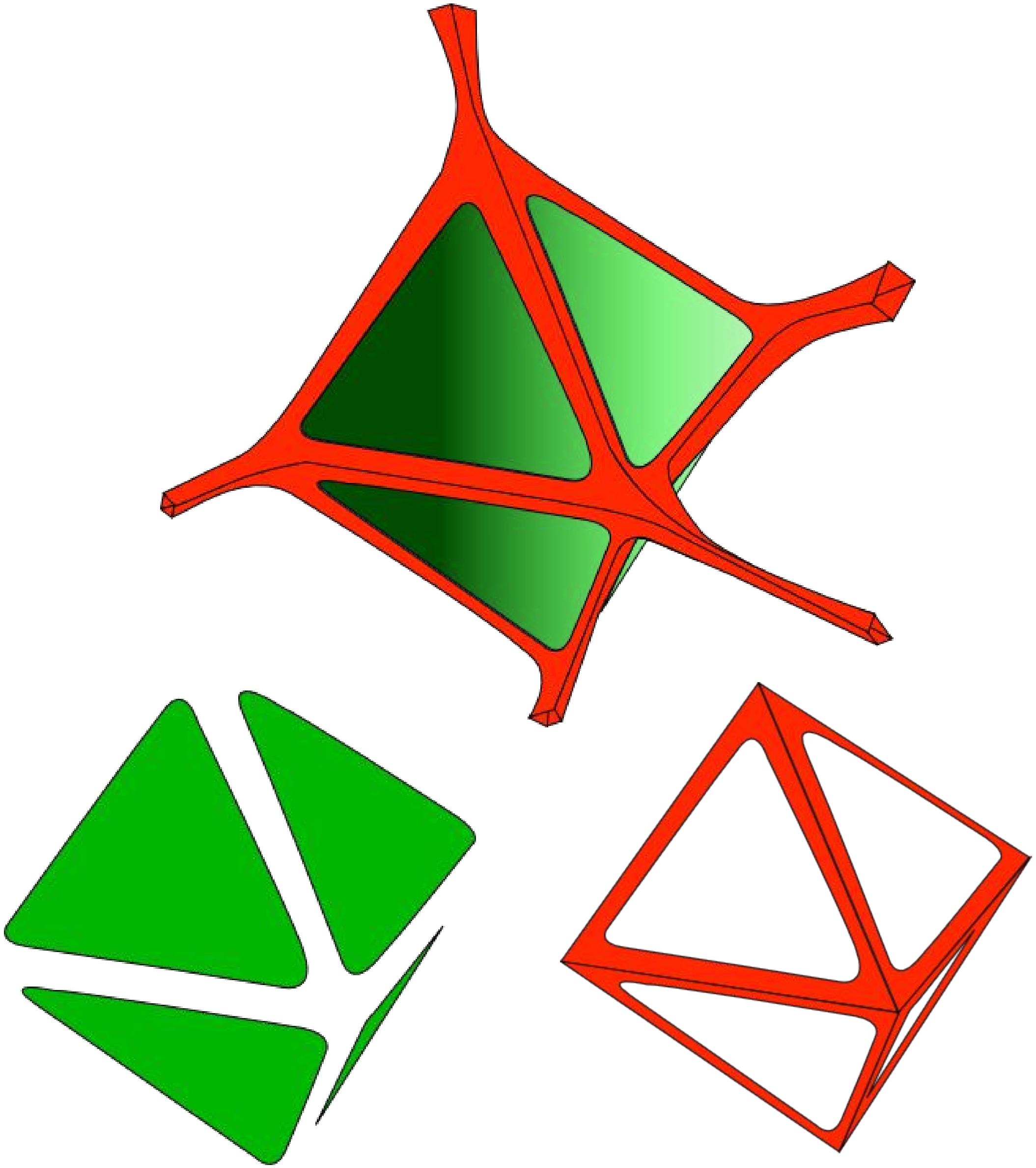

Microstructure

Within the grains and the melt

$$0 = \nabla \cdot \boldsymbol{u}$$

$$0 = \nabla \cdot \boldsymbol{T}$$

Boundary condition

$$\Delta \boldsymbol{T}^k \cdot \boldsymbol{n}^k = \gamma^k \left(\nabla \cdot \boldsymbol{n}^k \right) \boldsymbol{n}^k - \tilde{\nabla} \gamma^k$$

$$0 = \Delta \boldsymbol{u}^k$$

Kinematic relation

$$0 = \frac{\partial F^k}{\partial t} + \boldsymbol{u}^k \cdot \nabla F^k$$

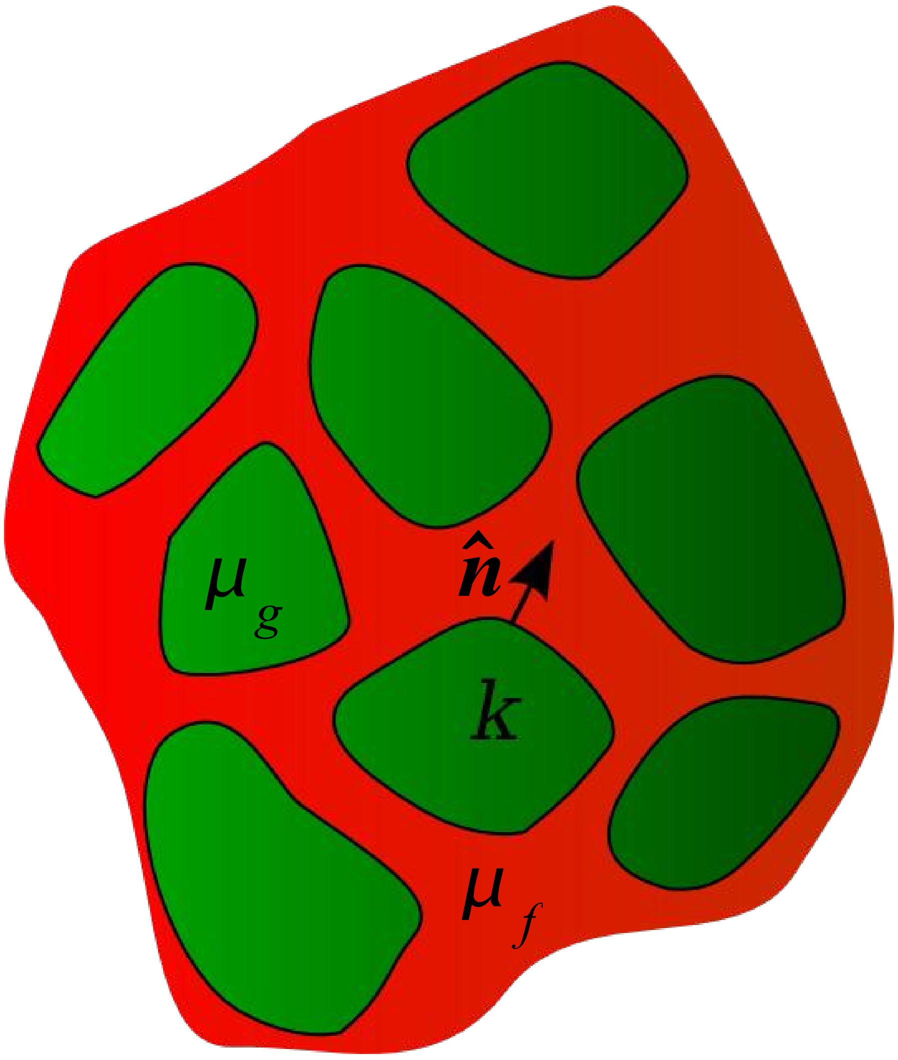

Midrange forces

Interaction between grains gives rise to variation in surface tension

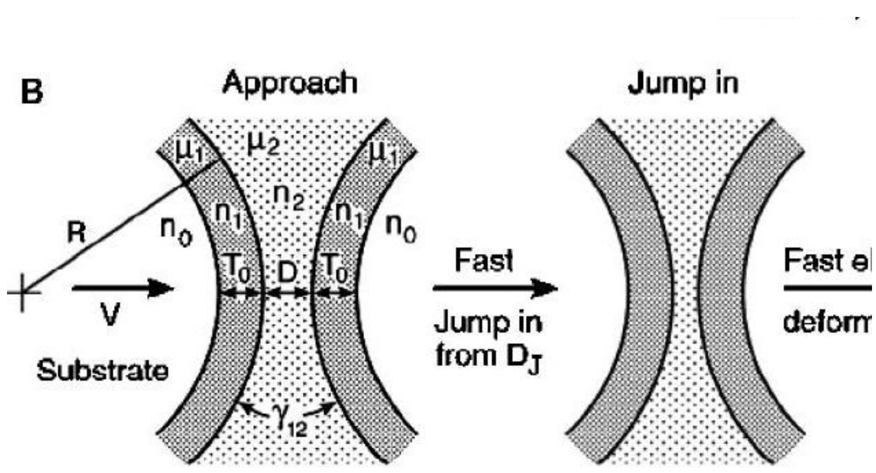

Chen et al.[2004]

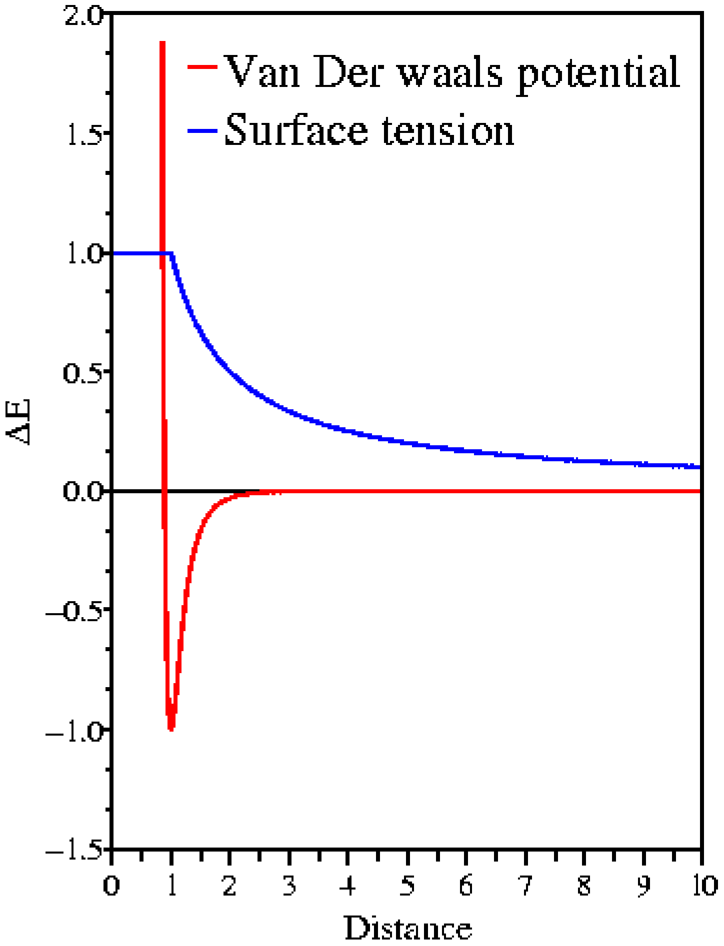

Steady-state grain shape

$$\boldsymbol{u}^g \cdot \boldsymbol{n} = 0$$

$$\boldsymbol{u}^m \cdot \boldsymbol{n} = 0$$

No-slip boundary condition

$$\boldsymbol{u}^g \cdot \hat{\boldsymbol{\theta}} - \boldsymbol{u}^m \cdot \hat{\boldsymbol{\theta}} = 0$$

$$\hat{\boldsymbol{\theta}} \cdot \Delta \boldsymbol{T} \cdot \boldsymbol{n} + \hat{\boldsymbol{\theta}} \cdot \tilde{\boldsymbol{\nabla}} \gamma = 0$$

Marangoni condition

$$\gamma = \gamma_0 + \sum_n \gamma_n P_n(\cos\theta)$$

$$F(r,\theta) = r - a - \epsilon \sum_n f_n(\theta)$$

Steady-state grain shape

$$\frac{d}{d\theta}\left(\sin\theta \frac{d f_n}{d\theta}\right) = P_n(\cos\theta)\sin\theta\left(2a - 3Ca\frac{\gamma_n a^2\left[(n+1)\lambda + n\right]}{(1+\lambda)(2\mathrm{n}+1)}\right)$$

Faceting during sintering

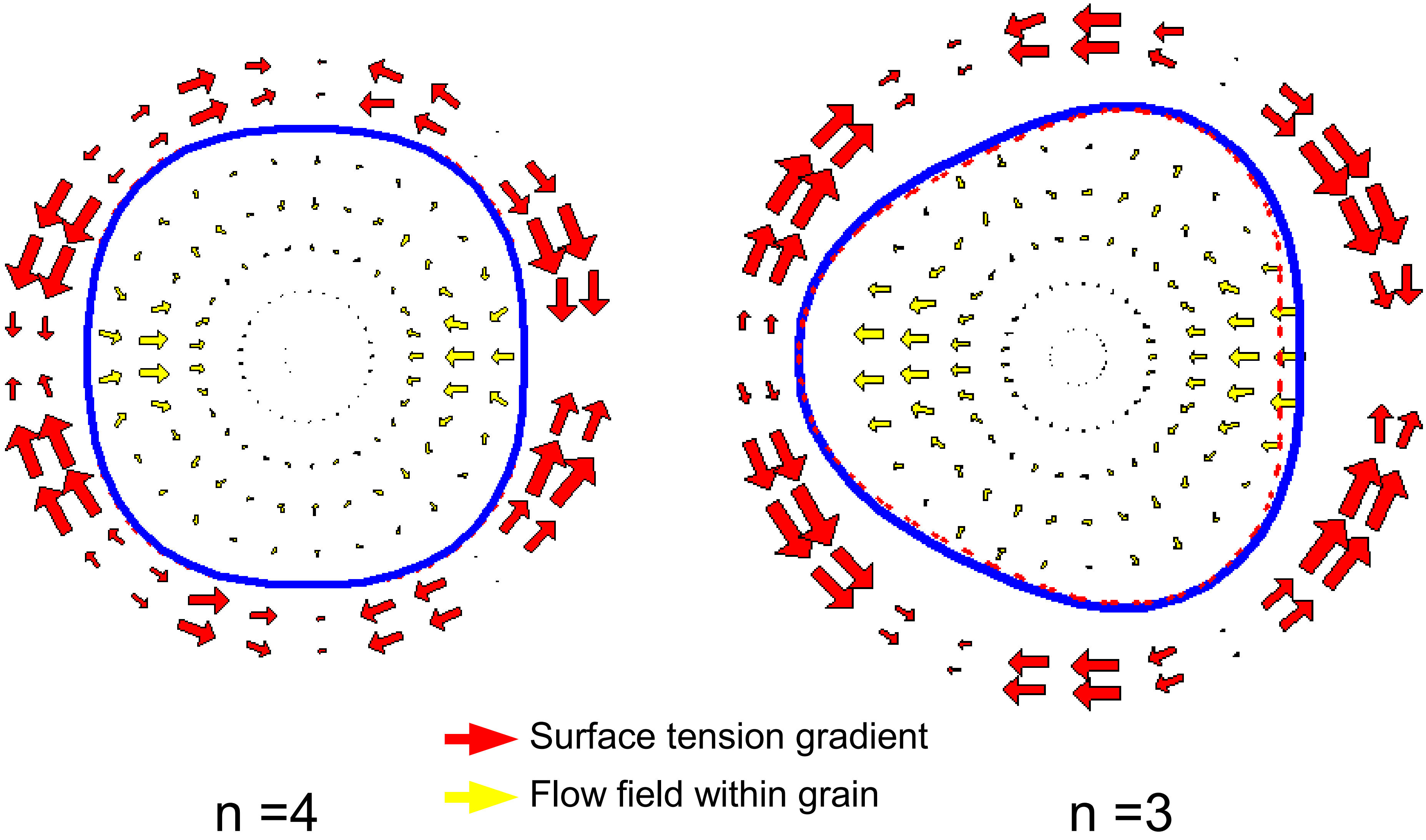

Numerical solution

$$
\begin{aligned}
\boldsymbol{u}^{\boldsymbol{i}}(\boldsymbol{r}_{\mathbf{0}}) &= \frac{2}{1+\lambda}\left[\boldsymbol{u}^{\infty}(\boldsymbol{r}_{\mathbf{0}}) - \frac{1}{4\pi Ca}\sum_k \int_{\Gamma^k} \Delta \boldsymbol{f}^{\boldsymbol{k}}(\boldsymbol{r})\cdot\boldsymbol{J}(\boldsymbol{r},\boldsymbol{r}_{\mathbf{0}})\,d\Gamma^k\right] \\
&\quad + \frac{(1-\lambda)}{\pi(1+\lambda)}\sum_k \int_{\Gamma^k} \boldsymbol{n}^{\boldsymbol{k}}\cdot\boldsymbol{K}(\boldsymbol{r},\boldsymbol{r}_{\mathbf{0}})\cdot\boldsymbol{u}^{\boldsymbol{k}}(\boldsymbol{r})\,d\Gamma^k \\
0 &= \frac{\partial F^k}{\partial t} + \boldsymbol{u}^{\boldsymbol{k}}\cdot\boldsymbol{\nabla} F^k \\
\boldsymbol{J}(\boldsymbol{r},\boldsymbol{r}_{\mathbf{0}}) &= -\boldsymbol{I}\ln(|\boldsymbol{r}-\boldsymbol{r}_{\mathbf{0}}|) + \frac{(\boldsymbol{r}-\boldsymbol{r}_{\mathbf{0}})(\boldsymbol{r}-\boldsymbol{r}_{\mathbf{0}})}{(|\boldsymbol{r}-\boldsymbol{r}_{\mathbf{0}}|)^2} \\
\boldsymbol{K}(\boldsymbol{r},\boldsymbol{r}_{\mathbf{0}}) &= -4\frac{(\boldsymbol{r}-\boldsymbol{r}_{\mathbf{0}})(\boldsymbol{r}-\boldsymbol{r}_{\mathbf{0}})(\boldsymbol{r}-\boldsymbol{r}_{\mathbf{0}})}{(|\boldsymbol{r}-\boldsymbol{r}_{\mathbf{0}}|)^4}
\end{aligned}
$$

Nondimensional parameters

$$\lambda = \frac{\mu_g}{\mu_m}$$

$$Ca = \frac{\mu_m u_0}{\gamma_0}$$

$$\psi = \frac{A_{gg}}{A_{gg} + A_{gm}}$$

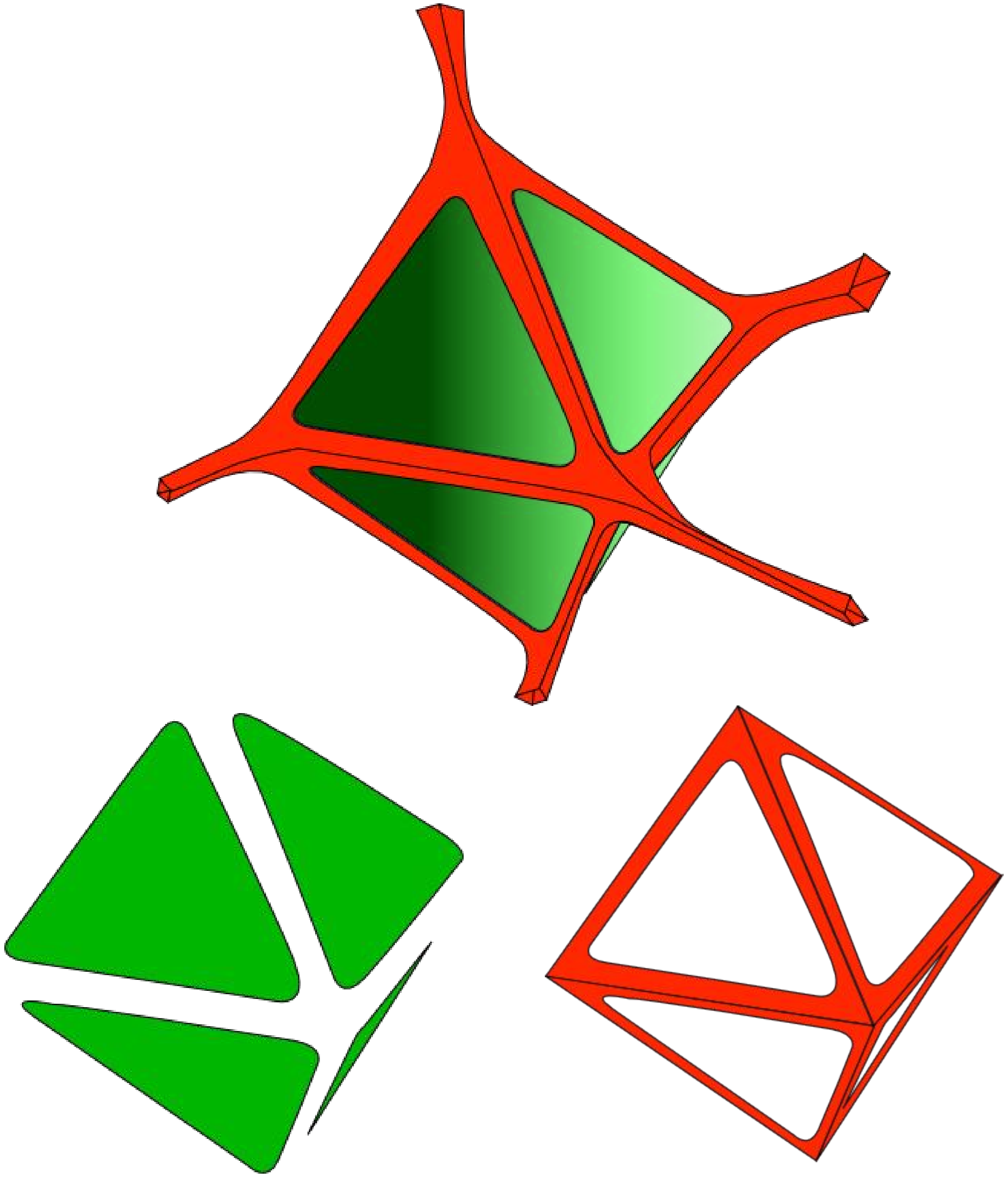

Boundary Elements Model

- Discretizing the BIE
- Evaluating singular integrals
- Updating the position of Lagrangian marker points

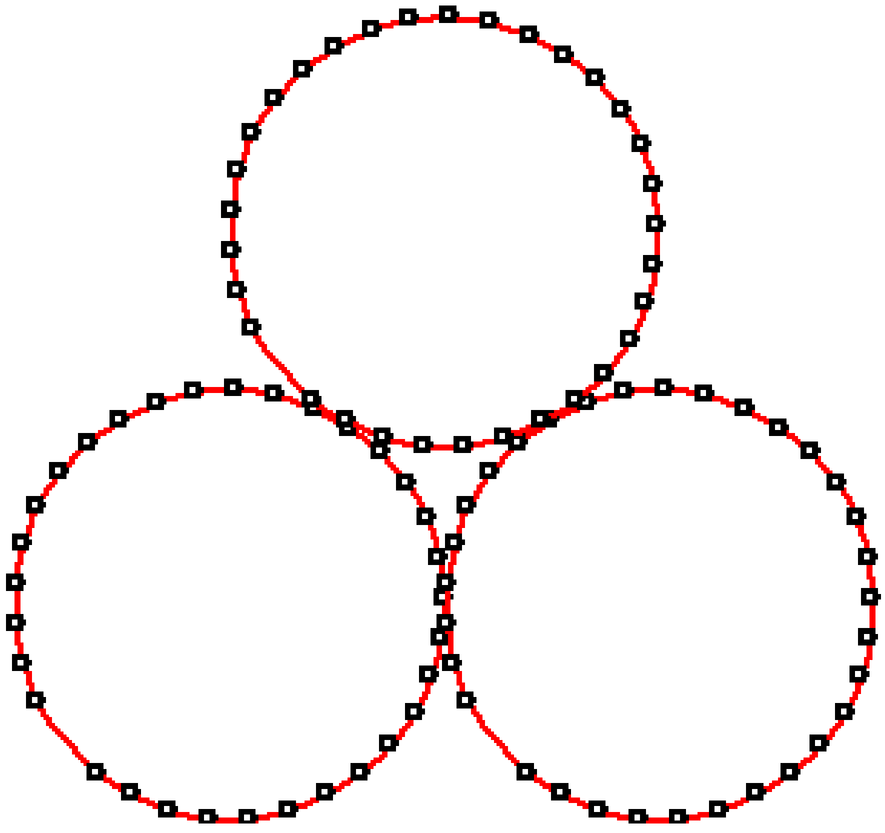

Discretization

- Collocating the poles at nodes
- Cubic spline interpolation of position, allows analytical evaluation of tangent, normal, and curvature
- Linear interpolation of the velocity field

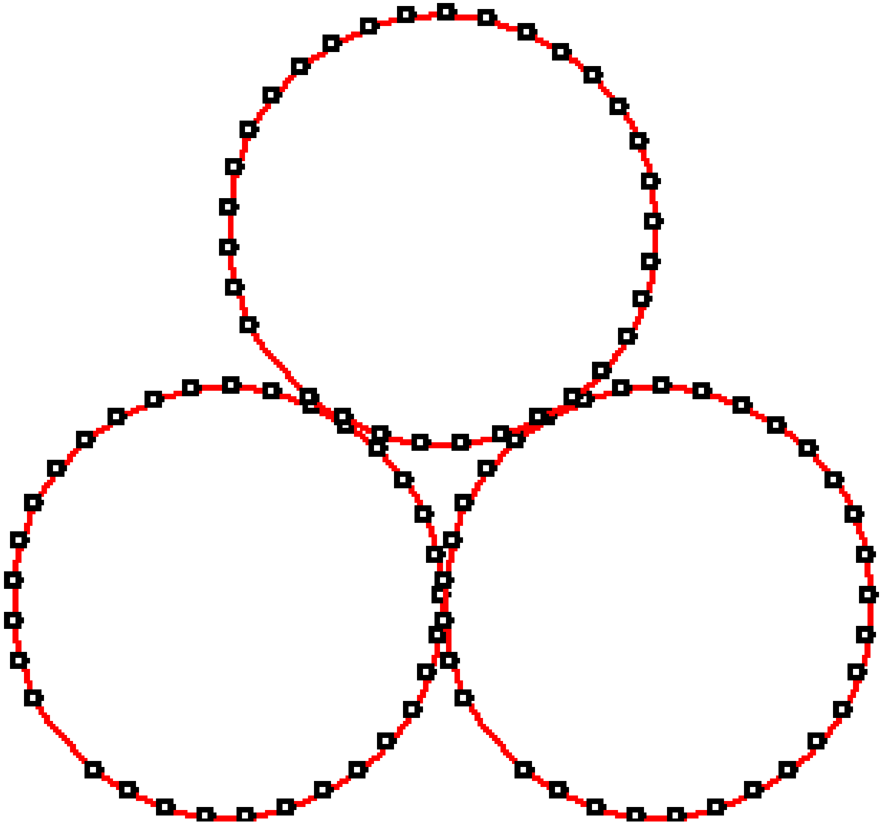

Integral evaluation

- Gaussian quadrature within nonsingular elements
- Radial integration method *[Gao, 2006]*, within singular elements
- Velocity optimized using a quadratic optimization scheme to ensure

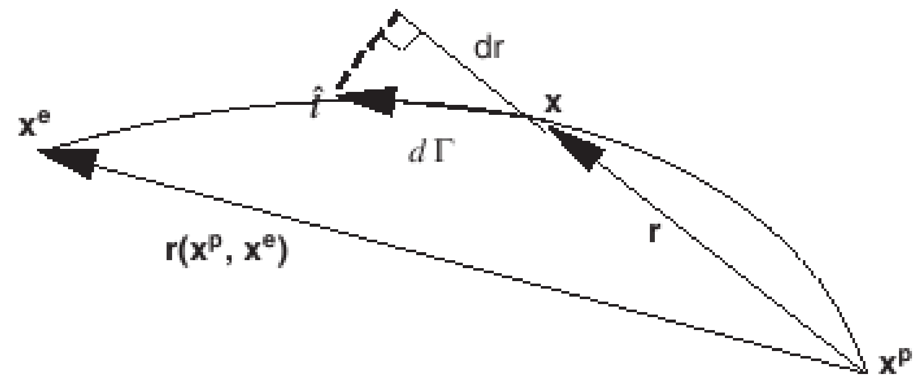

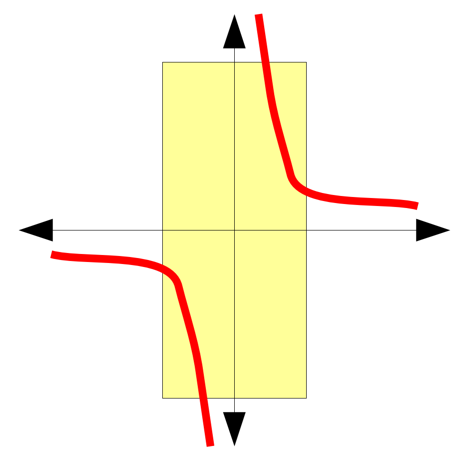

$$\boldsymbol{u} \cdot \boldsymbol{n} = 0$$

Updating shape

- Update nodal coordinates using forward Eulerian integration
- Remove high curvature nodes
- Marker position updated until convergence is attained

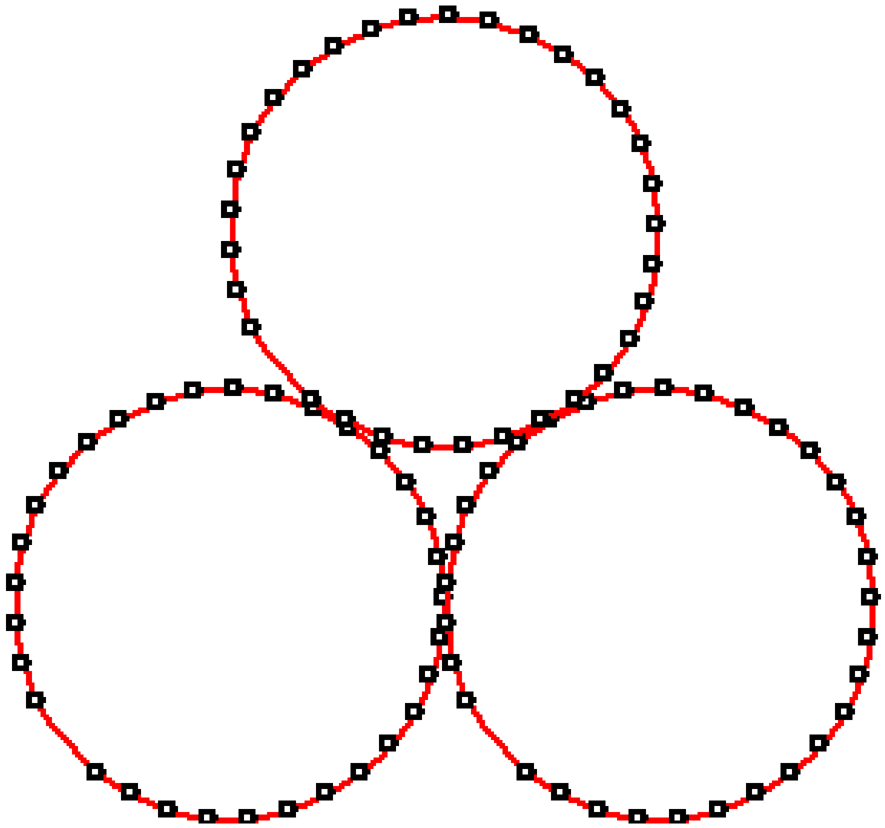

Contiguity

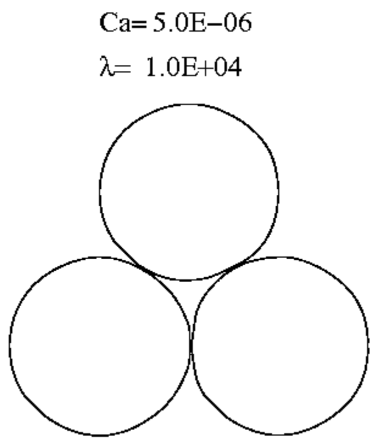

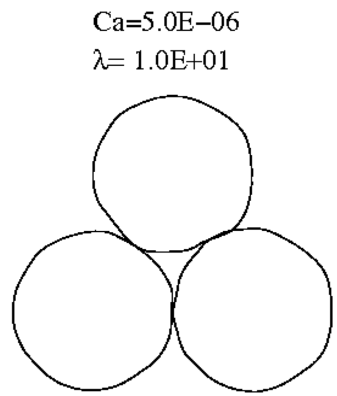

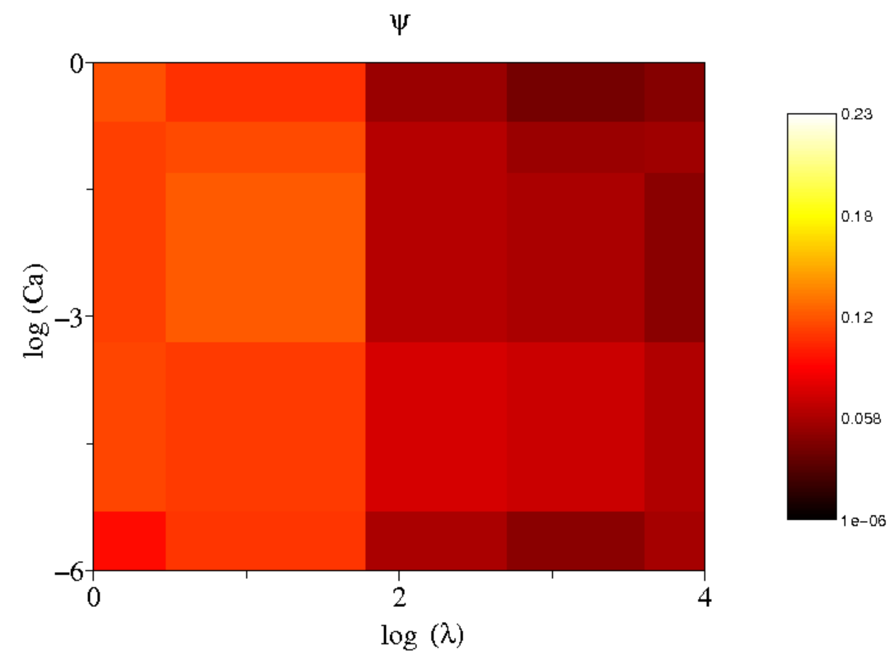

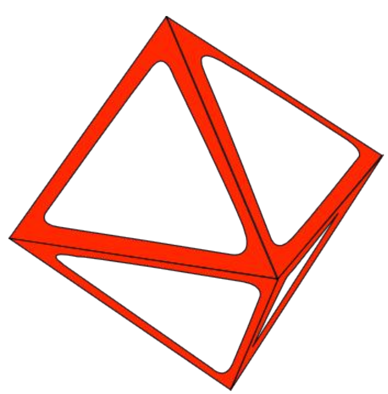

$$\psi = \frac{A_{gg}}{A_{gg} + A_{gm}}$$

Hier-Majumder *[2008]*

Contiguity and elastic properties

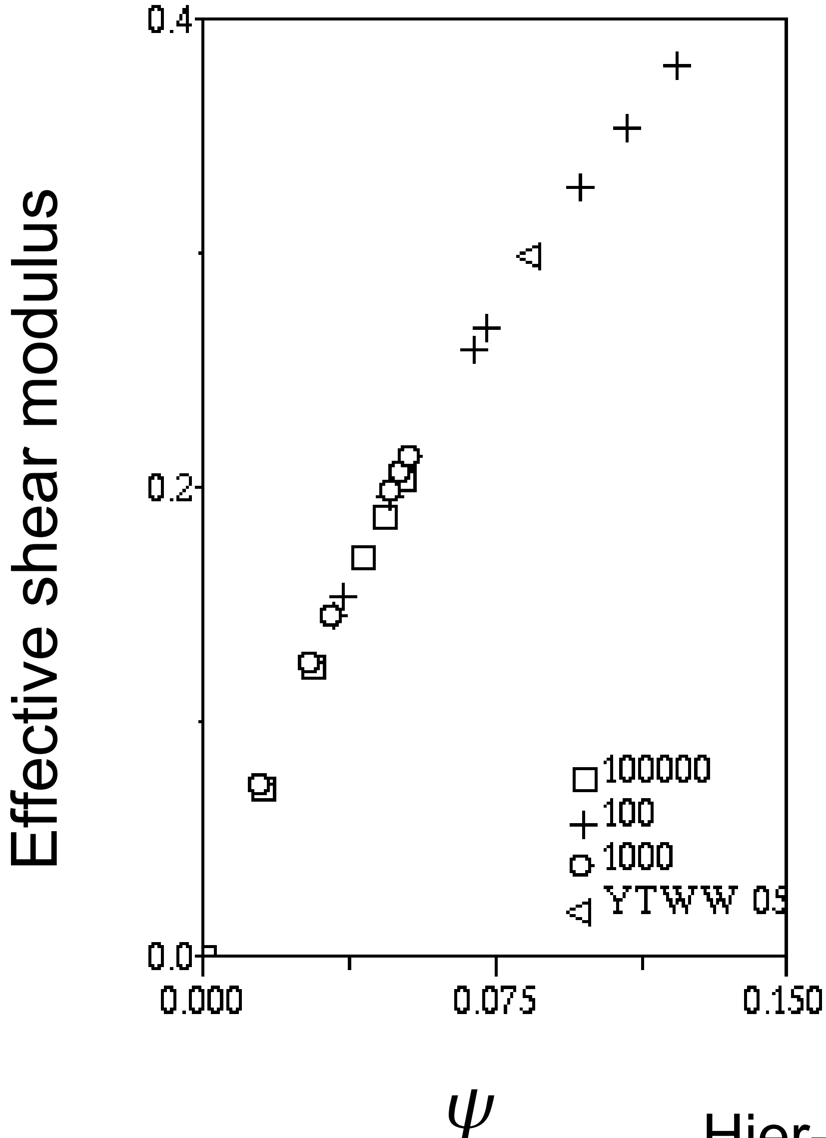

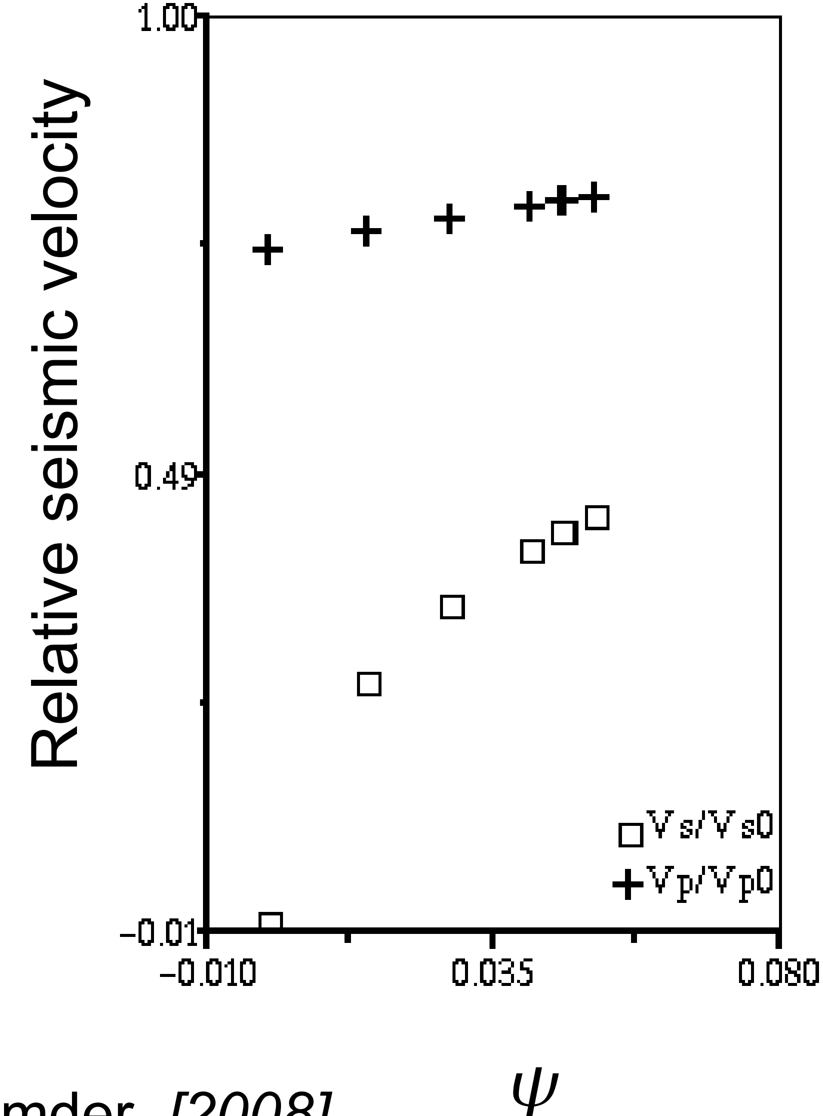

Hier-Majumder *[2008]*

Viscosity and elastic properties

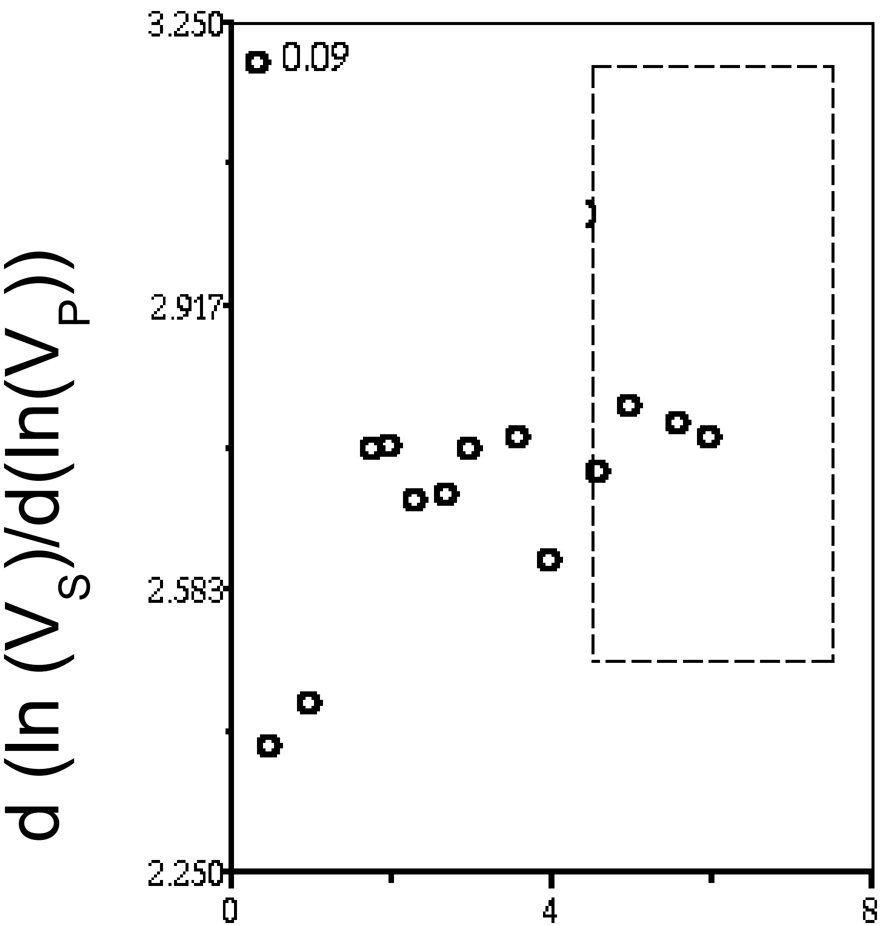

$\log(\lambda)$

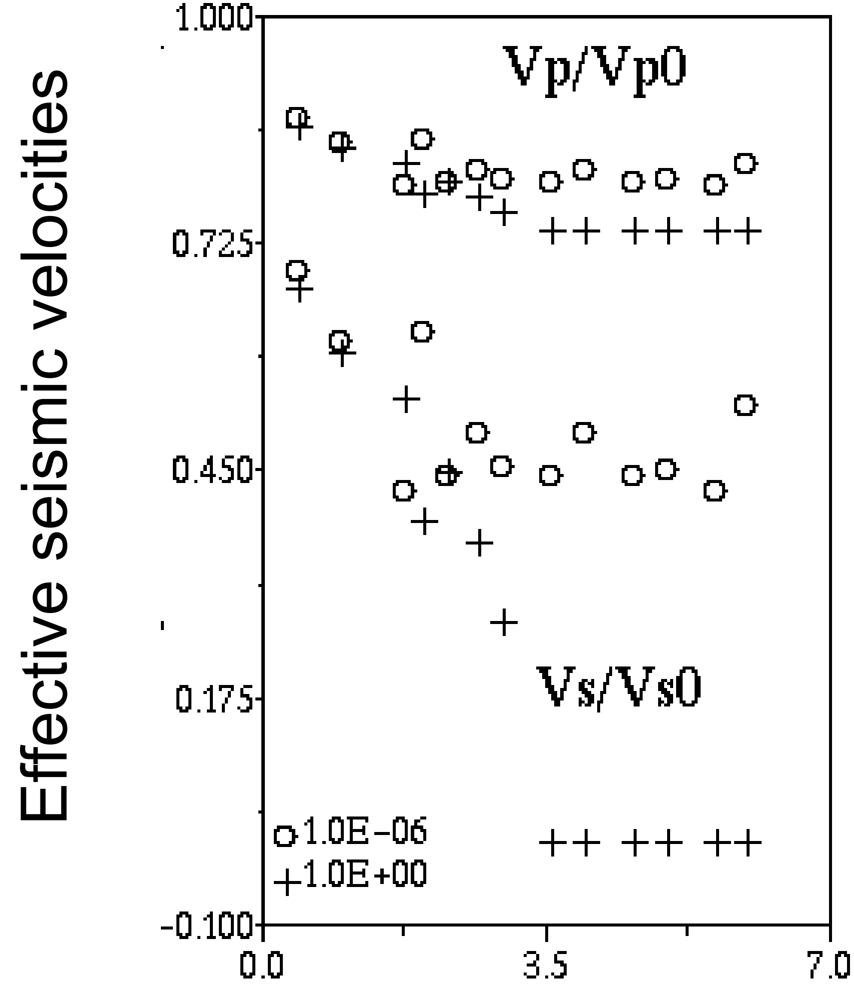

$\log(\lambda)$

Hier-Majumder *[2008]*

Contiguity and melt fraction

$$\psi = 1 - A\sqrt{\phi}$$ (at a given viscosity ratio)

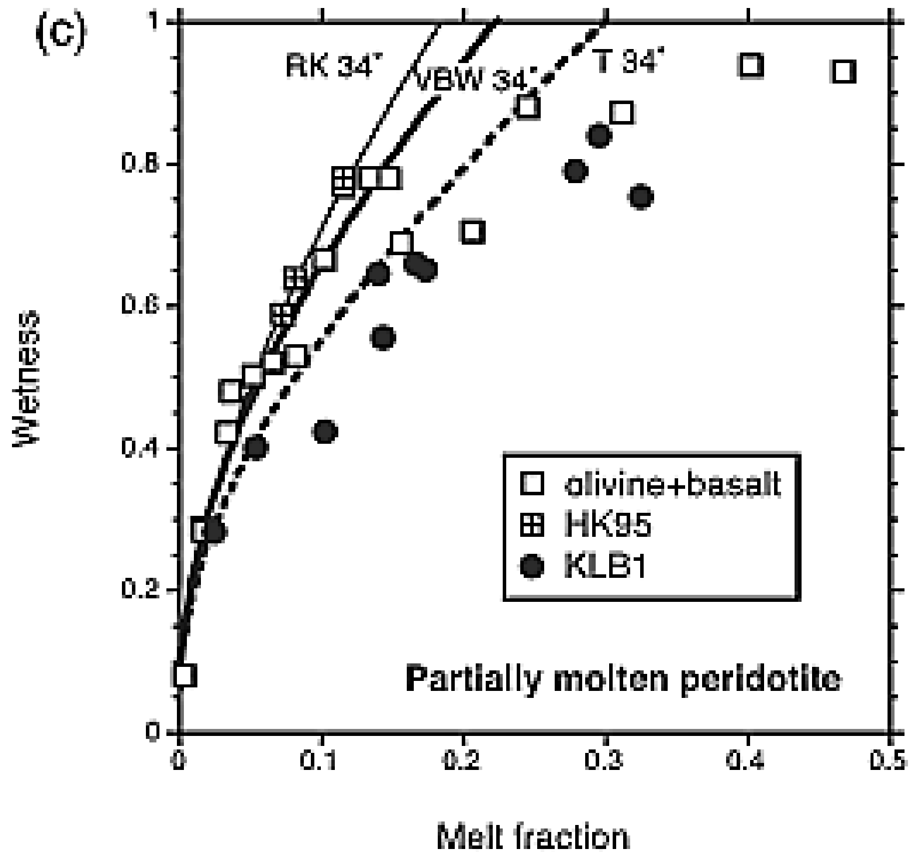

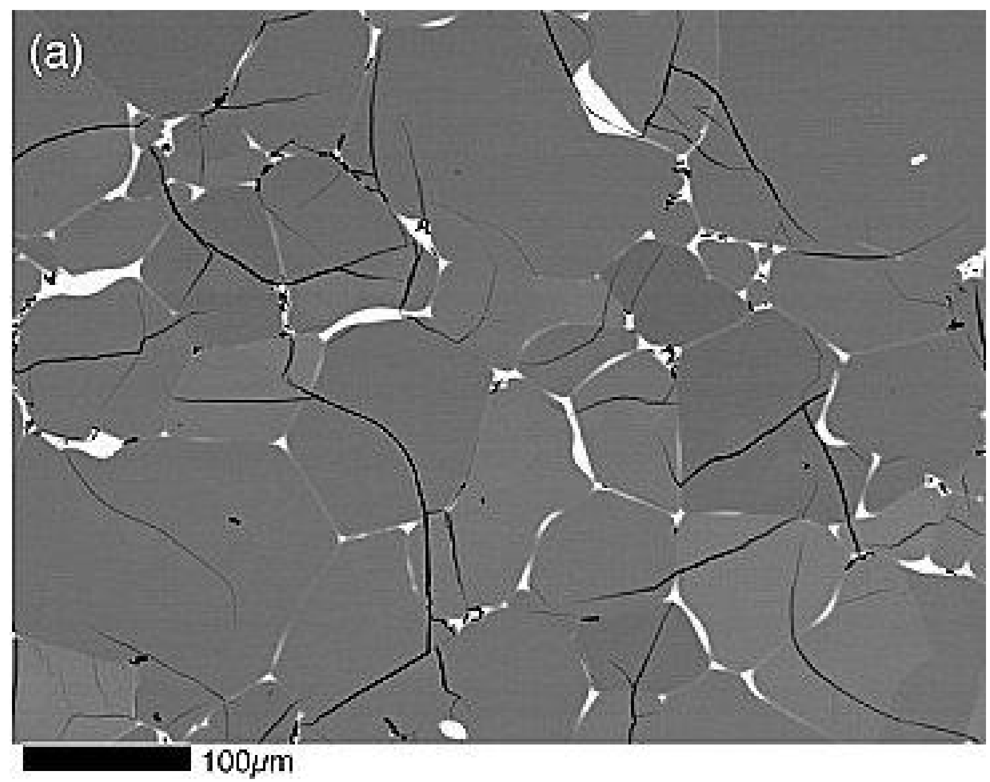

Yoshino *et a*l [*2005*]

Extent of melting in the ULVZ

- Estimate from inclusion models 5-30 volume % melt for 3:1 reduction of shear and P wave velocities

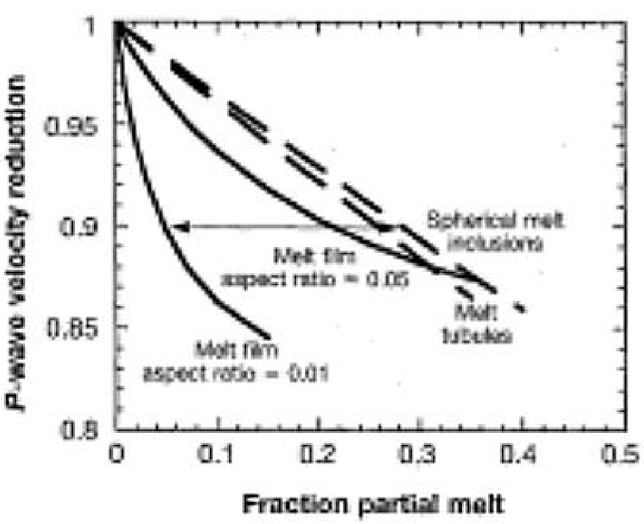

Williams and Garnero *[1996]*

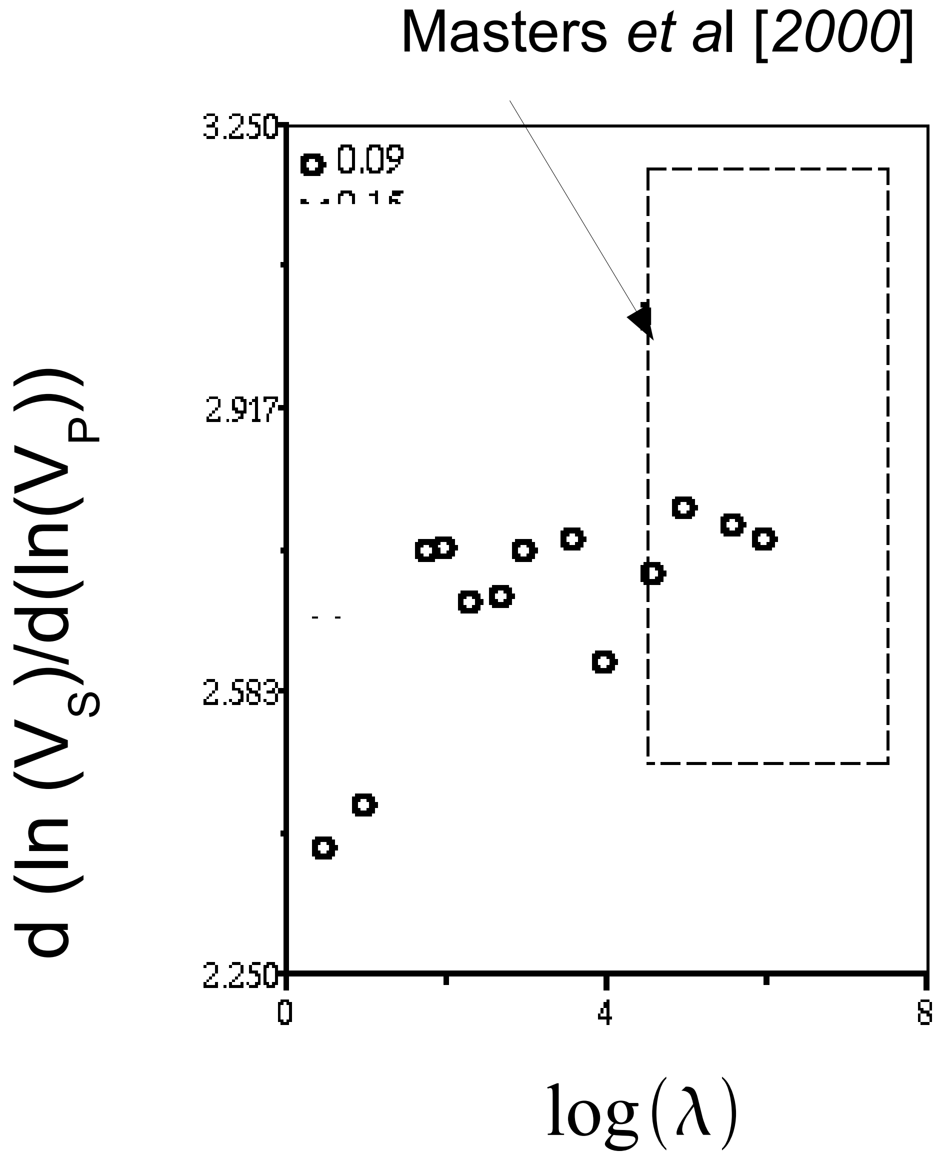

Hier-Majumder *[2008]*

Extent of melting in the ULVZ

- Current model indicates between 10-15% melting for 3:1 reduction of S and P wave velocities
- The ULVZ is molten, but probably not disaggregated

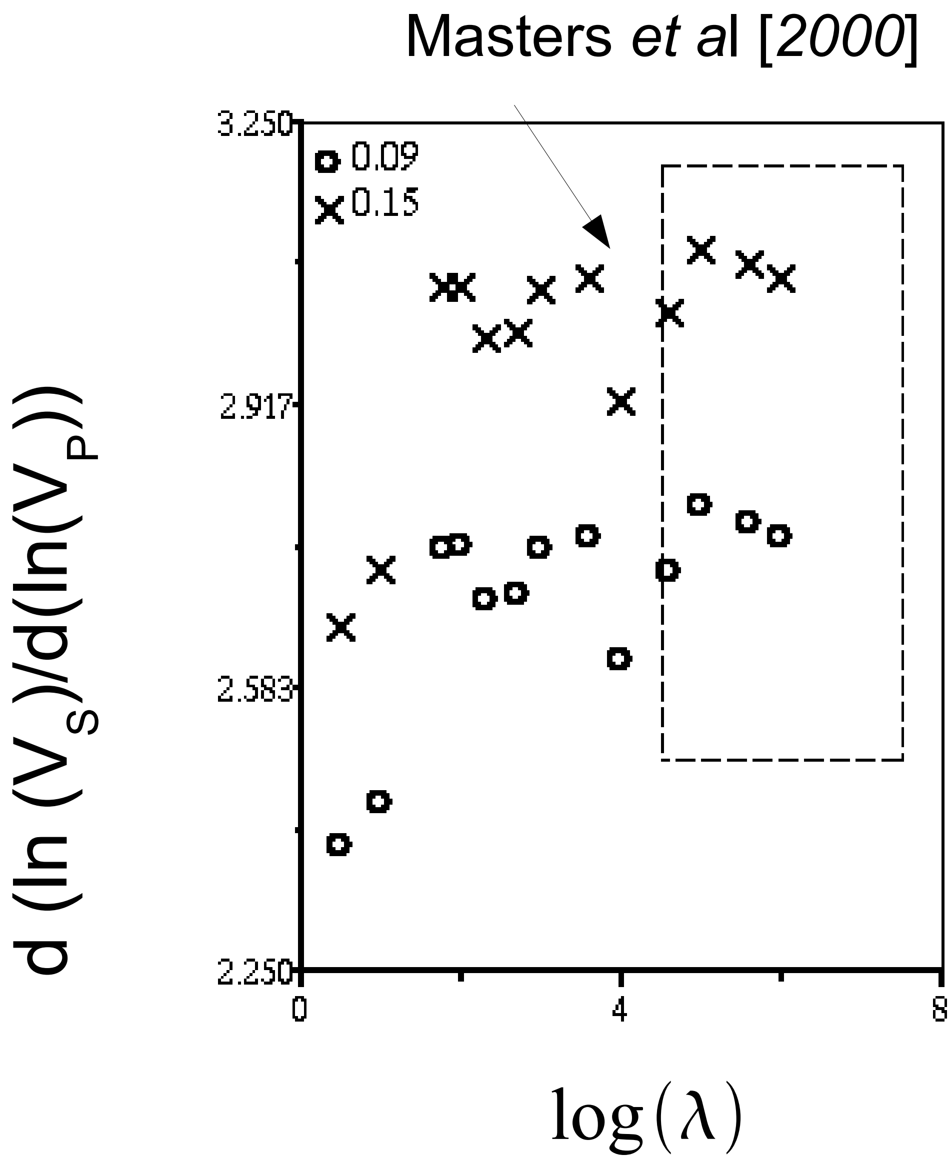

Hier-Majumder [2008]

Influence of melting on the topography of the ULVZ

- Coupled effect of surface tension, compaction, buoyancy, and deformation
- Mantle flow and viscosity contrast between the ULVZ and the ambient mantle

Two-phase theory

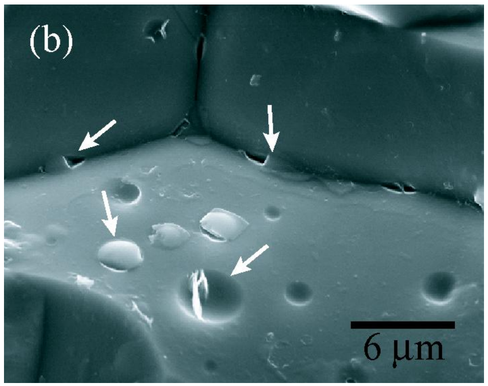

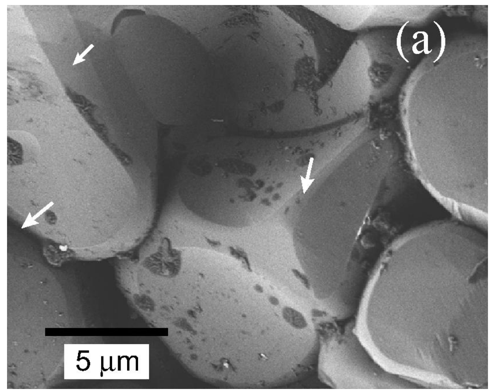

- Coupled viscous flow of the melt and the matrix
- Surface tension balance pressure, viscous stress, and body forces
- Incorporates both melt geometry and disaggregation.

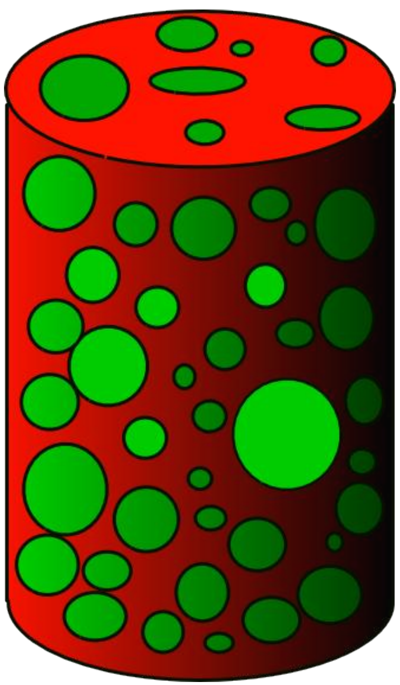

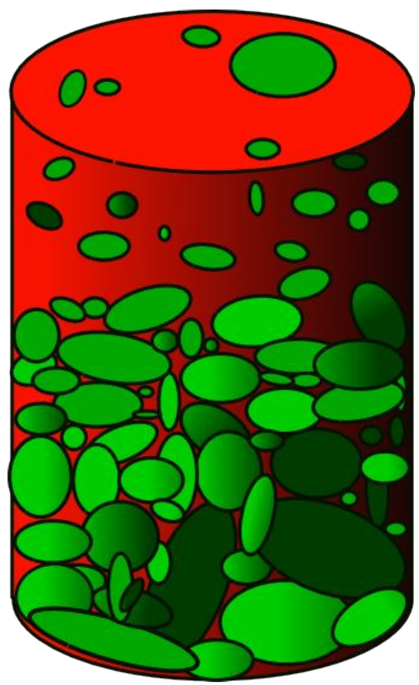

Governing equations (1D)

Conservation of Mass

$$\frac{\partial \phi}{\partial t} = \frac{\partial}{\partial y}\left((1-\phi) w\right)$$

Force balance (‘action-reaction’)

$$\xi (1-\phi) \frac{\partial^2 \chi}{\partial \phi^2}\left(\frac{\partial \phi}{\partial y}\right) + \frac{4}{3}\frac{\partial}{\partial y}\left(\frac{1-\phi^2}{\phi}\frac{\partial w}{\partial y}\right) - R(1-\phi) - \frac{4}{3}\frac{w}{\phi^2} = 0$$

Stress drop condition

$$\frac{\partial \chi}{\partial \phi} = -\Delta P + B \frac{D_m \phi}{D t}$$

Bercovici *et al. [2001]*

Some parameters

$$\xi = \frac{\gamma_{gm}\alpha_0}{\rho_s g \delta_s}$$

Modulates surface tension

$$R = \frac{\Delta \rho}{\rho_s}$$

Controls buoyancy

$$\delta_s = \sqrt{\frac{4\mu_s}{3c}}$$

Compaction length of the solid

Distribution of a neutrally buoyant melt layer

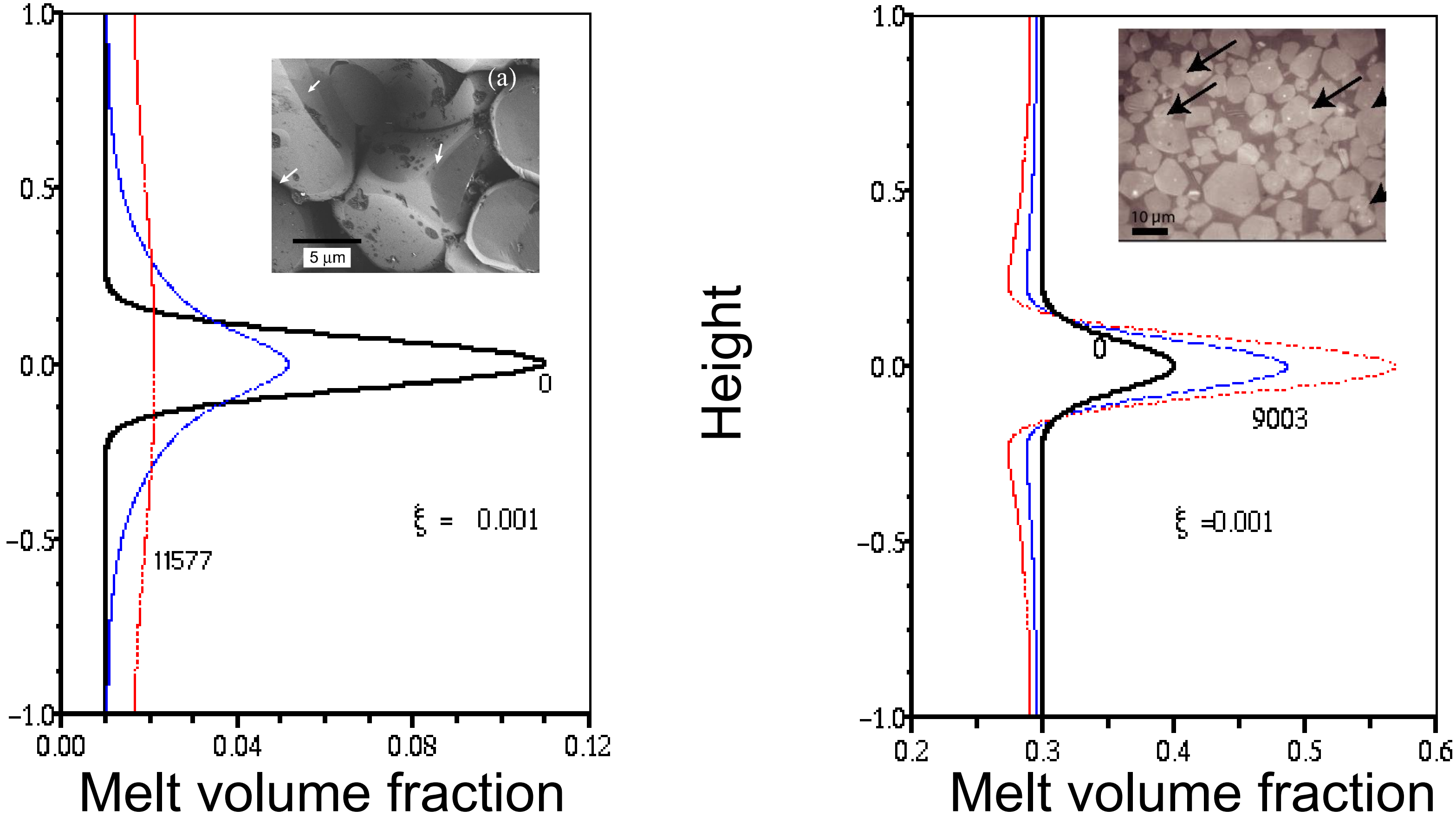

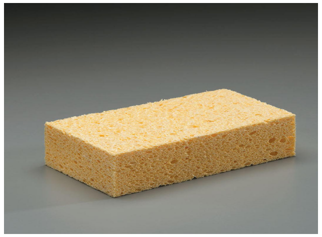

Hier-Majumder *et al* [*2006*]

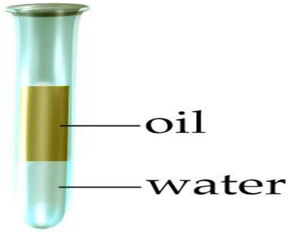

Storage of dense melt

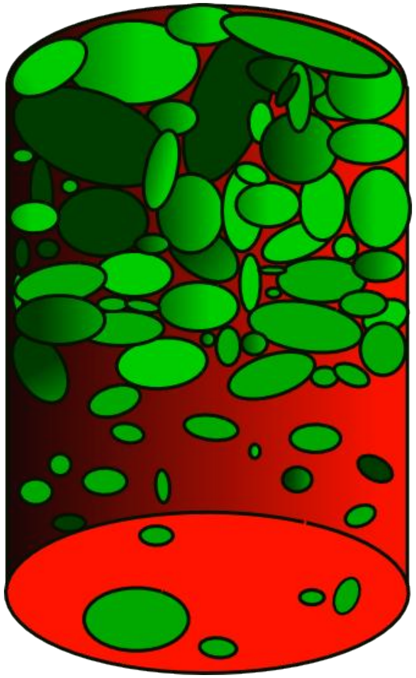

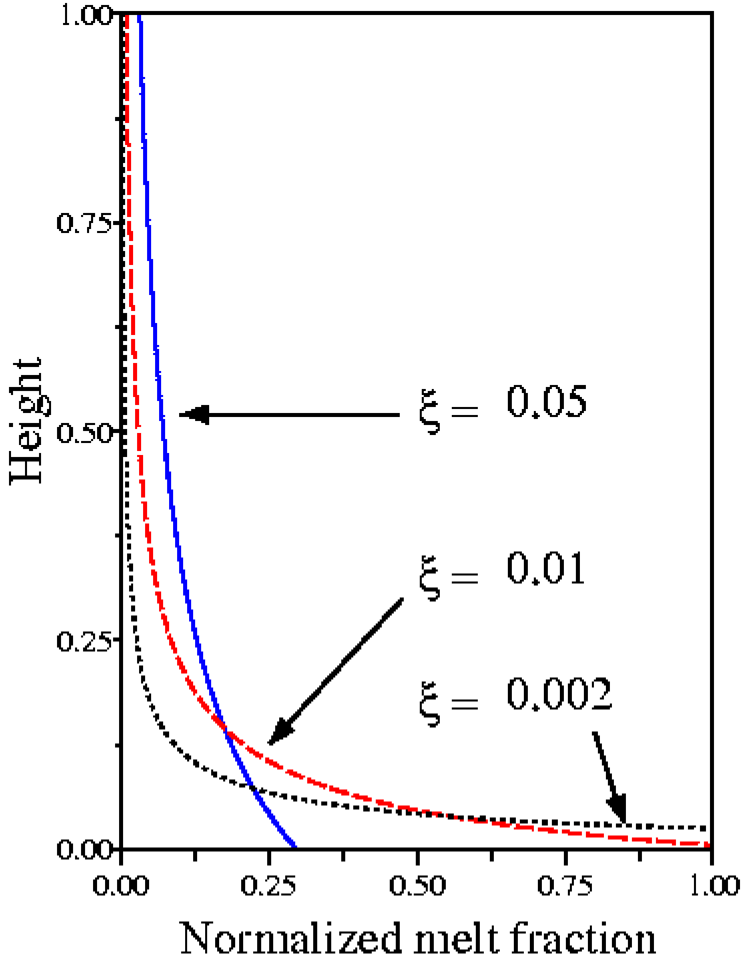

$$\xi = \frac{\gamma_{gm}\alpha_0}{\rho_s g \delta_s}$$

$$\delta_s = \sqrt{\frac{4\mu_s}{3c}}$$

Hier-Majumder *et al. [2006]*

Melt fraction and viscosity

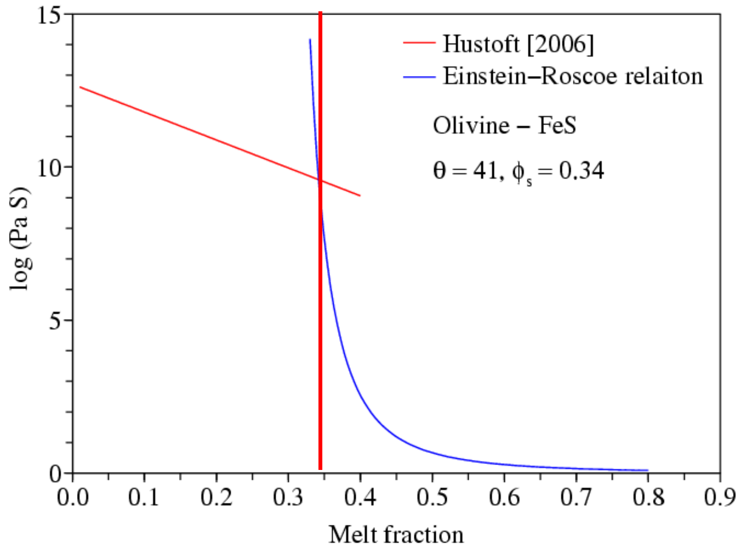

Figure 7

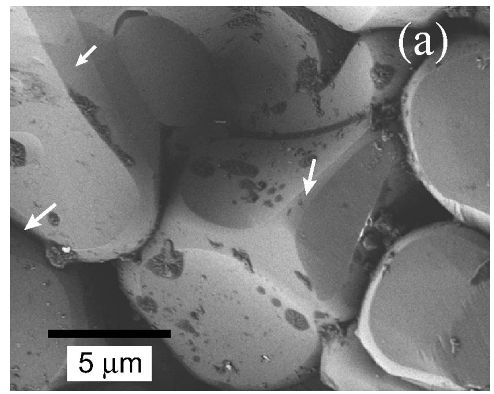

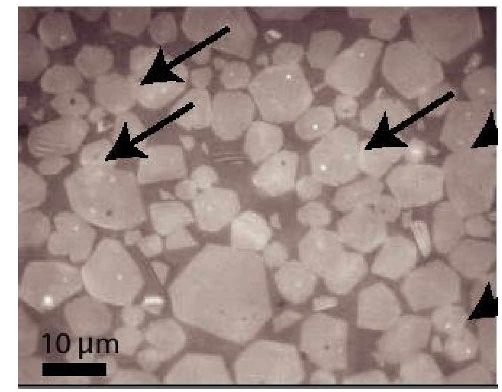

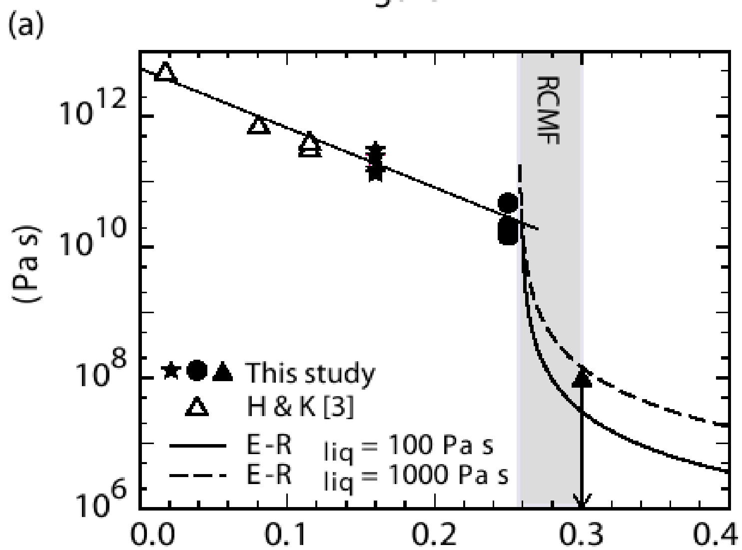

Scott and Kohlstedt, [2006].

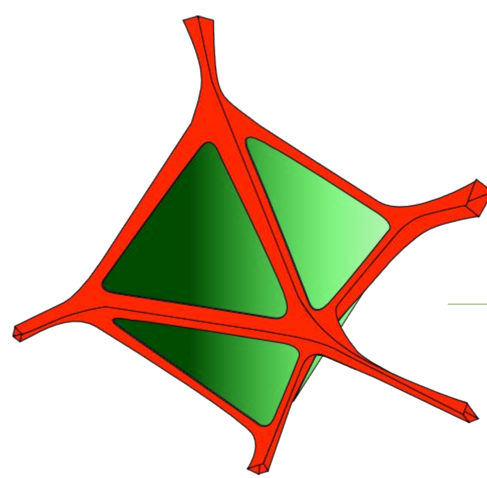

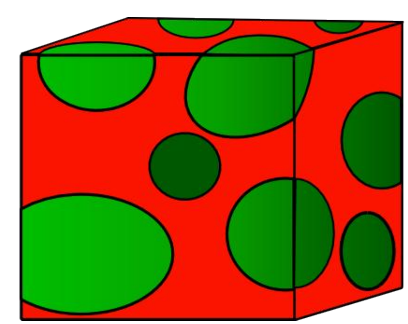

Low viscosity dense layer

Q = Sink strength

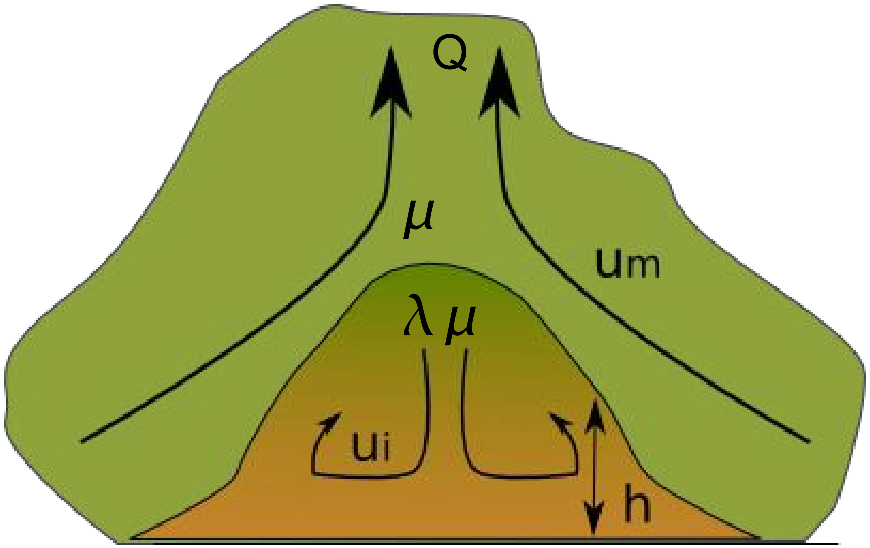

$$\tau^{i}_{r\theta} = \tau^{m}_{r\theta}$$

$$\boldsymbol{u}^{i}\cdot\hat{\boldsymbol{\theta}} = \boldsymbol{u}^{m}\cdot\hat{\boldsymbol{\theta}}$$

Boundary conditions

$$\hat{\boldsymbol{z}}\cdot\Delta\boldsymbol{T}\cdot\boldsymbol{n} = \Delta\rho g h$$

Topography relation

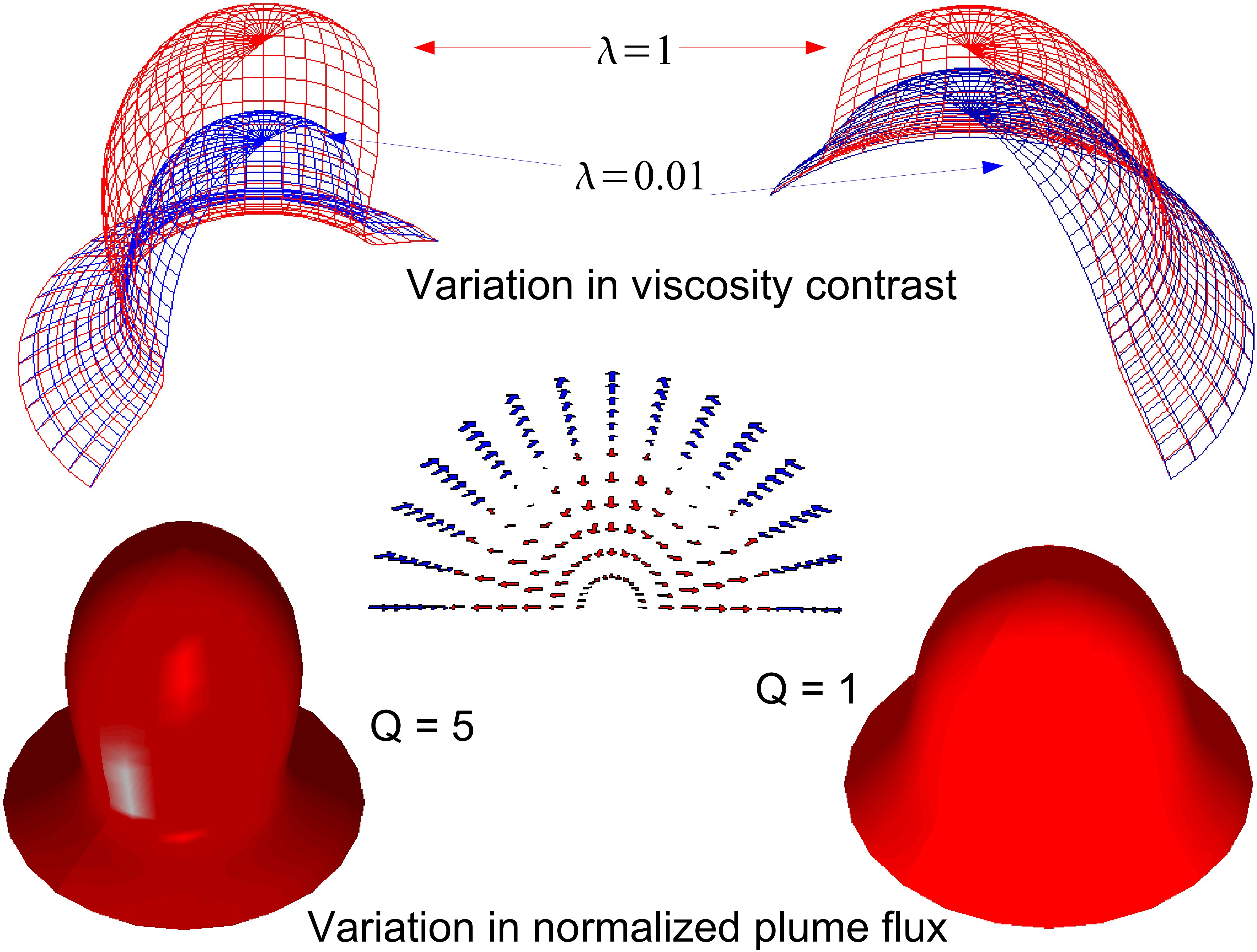

$\lambda = 1$
$\lambda = 0.01$
Variation in viscosity contrast
Q = 5
Q = 1
Variation in normalized plume flux

Conclusions

- Observed range of S and P-wave velocity changes can be explained by 10-15% melting
- The ULVZ is likely molten but not disaggregated
- Topography of the ULVZ is likely influenced by
  - Tension on grain boundaries
  - Plume flux
  - Density and viscosity contrast

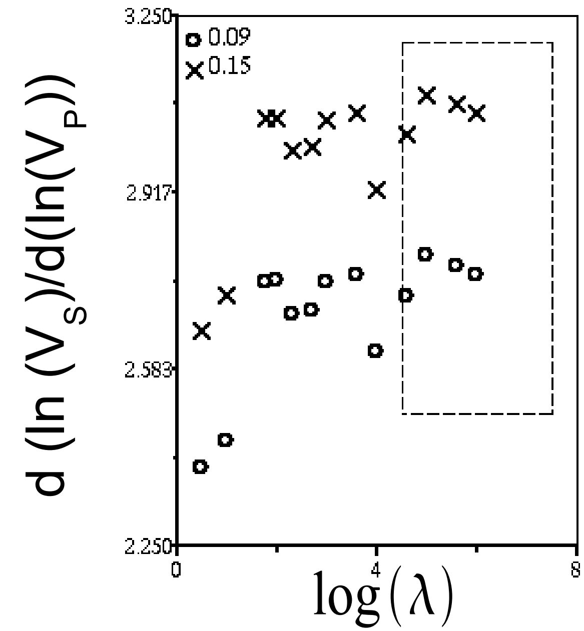

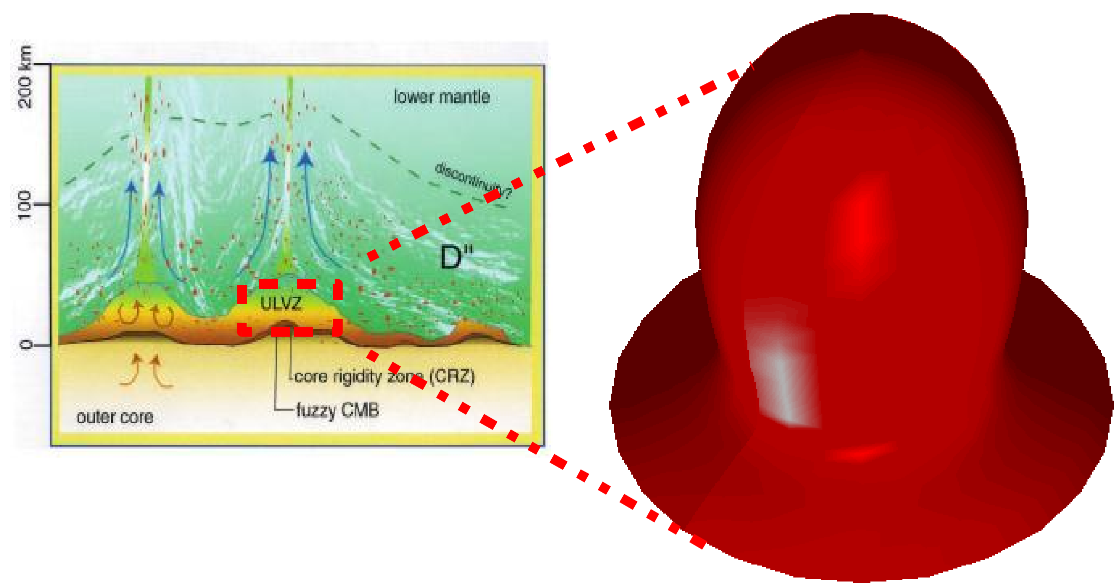

Lamb’s solution for a single particle

$$
\begin{aligned}
P(r,\theta) &= \sum_n p_n \\
u(r,\theta) &= \sum_n \left(\frac{(n+3)r^2 \boldsymbol{\nabla} p_n}{2\mu(n+1)(2\mathrm{n}+3)} - \frac{n\,\boldsymbol{r}\,p_n}{\mu(n+1)(2\mathrm{n}+3)} + \boldsymbol{\nabla}\Phi_n \right) \\
p_n &= a_n r^n P_n(\cos\theta) \\
\boldsymbol{\Phi}_n &= b_n r^n P_n(\cos\theta) \\
p_{-n-1} &= \frac{A_n}{r^{n+1}} P_n(\cos\theta) \\
\boldsymbol{\Phi}_{-n-1} &= \frac{B_n}{r^{n+1}} P_n(\cos\theta)
\end{aligned}
$$

Dihedral angle